Techno-Economic Analysis of a Novel Hydrogen-Based Hybrid Renewable Energy System for Both Grid-Tied and Off-Grid Power Supply in Japan: The Case of Fukushima Prefecture

Naoto Takatsu [1] and Hooman Farzaneh [1,2,*]

[1]   Interdisciplinary Graduate School of Engineering Sciences, Kyushu University, Fukuoka 816-8580, Japan; takatsu.naoto.917@s.kyushu-u.ac.jp
[2]   Platform of Inter/Transdisciplinary Energy Research, Kyushu University, Fukuoka 819-0395, Japan
*   Correspondence: farzaneh.hooman.961@m.kyushu-u.ac.jp

check for updates

Abstract: After the Great East Japan Earthquake, energy security and vulnerability have become critical issues facing the Japanese energy system. The integration of renewable energy sources to meet specific regional energy demand is a promising scenario to overcome these challenges. To this aim, this paper proposes a novel hydrogen-based hybrid renewable energy system (HRES), in which hydrogen fuel can be produced using both the methods of solar electrolysis and supercritical water gasification (SCWG) of biomass feedstock. The produced hydrogen is considered to function as an energy storage medium by storing renewable energy until the fuel cell converts it to electricity. The proposed HRES is used to meet the electricity demand load requirements for a typical household in a selected residential area located in Shinchi-machi in Fukuoka prefecture, Japan. The techno-economic assessment of deploying the proposed systems was conducted, using an integrated simulation-optimization modeling framework, considering two scenarios: (1) minimization of the total cost of the system in an off-grid mode and (2) maximization of the total profit obtained from using renewable electricity and selling surplus solar electricity to the grid, considering the feed-in-tariff (FiT) scheme in a grid-tied mode. As indicated by the model results, the proposed HRES can generate about 47.3 MWh of electricity in all scenarios, which is needed to meet the external load requirement in the selected study area. The levelized cost of energy (LCOE) of the system in scenarios 1 and 2 was estimated at 55.92 JPY/kWh and 56.47 JPY/kWh, respectively.

Keywords: hybrid renewable energy system; simulation; optimization; hydrogen; supercritical water gasification; Japan

1. Introduction

Japan is facing a severe challenge regarding the heavy dependence on fossil fuels after the Great East Japan Earthquake [1]. Fossil fuels currently account for 89% of the total energy consumption in Japan, which approaches the level of the oil shock in 1973. To tackle this challenge, the government of Japan needs to develop and utilize renewable energy sources to increase its energy self-sufficiency rate and reduce the environmental impacts of the increased use of fossil fuels [2,3]. Since renewable energies are from the natural environment, they are all weather-dependent, which makes them vulnerable in developing a stable power system. As a solution, hybridization of multiple renewable energy resources (RER) will allow us to provide reliable, durable, and cheaper electricity from using renewable technologies compared to the individual power generators such as solar photovoltaics or wind turbine, continuously and without interruption. Furthermore, when the hybrid renewable energy system

(HRES) is connected to a storage system such as battery or hydrogen storage, the excess energy generated by the renewable energies such as solar or wind can be stored and then utilized during the period when there is no sunshine and wind, wherein electricity is not being generated. Therefore, compared to a single renewable technology, the HRES works more efficiently in all weather conditions, indicating the pivotal role of the energy storage in this particular type of power system.

Although battery holds the most promise storage technology, there are several drawbacks with its limited lifespan and round-trip efficiency, in addition to the negative environmental impacts through its incorrect disposal. Hydrogen may be considered as an alternative with much higher storage capacity compared to batteries, which can be re-electrified in the HRES configuration. Besides electricity generation, hydrogen can also be burned as a fuel to provide additional thermal load, which results in reducing the levelized cost of energy (LCOE) generated form the HRES. Depending on the design and configuration of a hydrogen-based HRES, manufacturers can produce hydrogen by using a variety of technologies such as solar electrolysis of water, thermochemical water splitting, gasification of biomass, or even metabolic techniques such as biochemical and fermentation processes.

Among all technologies mentioned above, the conventional biomass gasification process is the most reasonable one for producing hydrogen in the HRES applications. However, to increase the hydrogen production efficiency, the pre-treatment and drying process should be considered in this method. One of the recent advancements in hydrogen production is the hydrothermal gasification of biomass feedstock, in which water is being used as the gasifying agent over its supercritical condition (374 °C and 22.1 MPa). The Supercritical Water Gasification (SCWG) has shown significant improvement in the overall yield of the gasification process and hydrogen production [4–8]. The generated syngas from the SCWG includes a mixture of carbon monoxide and methane, which can be burned in an auxiliary fired heater to provide the amount of thermal energy needed in securing the gasification temperature of 650 °C. The SCWG decomposes biomass feedstock entirely, without using any pre-treatment system for residue and wastewater [9].

Research that concentrates on the techno-economic analysis of the hydrogen-based HRES has drawn the attention of global scholars. The current and past investigations have demonstrated a variety of analytical methods used to address the optimal design and configuration of the hydrogen-based HRES. Chang et al. discussed the economic analysis of the integration of a biomass fermentation with the HRES, consisting of the Photovoltaic (PV) module, wind turbine, electrolyzer, and fuel cell [10]. The proposed system can work as a stand-alone Bio-HRES, generating about 31 MWh per annum electric power, together with providing the thermal energy, and hydrogen at a LCOE of 0.793 USD/kWh. Sharifi et al. discussed the optimal design of a hydrogen-based HRES, using the particle swarm optimization (PSO) method, in order to minimize the total cost of the system and CO_2 emissions [11]. Their proposed system consists of a solar water electrolyzer coupled with a wind turbine, a diesel generator, a battery bank, and a fuel cell. The total cost of the system was estimated at EUR 93,487 over 25 years lifespan of the system. Table 1 shows a summary of the recent hydrogen-based HRES studies with the different modeling approaches used in their techno-economic analysis.

Table 1. Summary review on hydrogen-based hybrid renewable energy system (HRES) configuration and modeling approaches.

System Components								Objective Function	Method	Ref
WT	PV	FC	Biomass	Battery	H2 Tank	Electrolyzer	Diesel Other			
✔	✔	✔		✔	✔	✔	✔	Total Cost/CO_2 Emission/unmet load	PSO [1]	[12]
✔	✔	✔		✔	✔	✔	✔	total cost	SA [2]	[13]
✔	✔	✔		✔	✔	✔	✔	Total cost/CO_2 Emission/unmet load	GA [3]	[14]
✔	✔	✔			✔	✔	✔	Total cost/CO_2 Emissions/unmet load	FL [4]	[15]
✔		✔	✔	✔	✔			LCOE	LP [5]	[16]
✔	✔	✔	✔	✔	✔			Annualized cost	GA	[17]
✔	✔	✔		✔	✔	✔	✔	Total cost	GA	[18]

[1] Particle swarm optimization; [2] simulated annealing; [3] genetic algorithm; [4] fuzzy logic; [5] linear programming.

The combination of biomass gasification with hybrid systems is gaining significant attention from the scientific community. All these studies focus on the gasification of relatively dry biomass combined with fuel cell hybrid systems [19–25]. The combination of SCWG and fuel cells is a new concept. However, research has been absent into integrated SCWG fuel cells in the literature, forming the basis of this study.

Following the previous studies, this paper aimed to optimally design a hydrogen-based HRES, consisting of a combination of the solar water electrolysis process, as the conventional method of hydrogen production, with the SCWG, as a more recent hydrogen production technology. The main electric power generators in the proposed HRES are solar panels and the fuel cell. Surplus power generated by the solar panels is consumed by an electrolyzer to produce hydrogen through the water decomposition process. The hydrogen is then stored in a hydrogen tank. The fuel cell performs as the backup system to generate electricity from the hydrogen when sunshine is not available. The SCWG is used to produce extra hydrogen in order to offset hydrogen deficiency in the hydrogen tank, using supercritical water as the reaction medium for the hydrothermal dissociation of the wet biomass feedstock. Residential food waste, with moisture content up to 40%, was considered as the possible feedstock to be used in the SCWG.

In this study, hydrogen is considered as functioning as an energy storage medium by storing renewable energies until the fuel cell converts it to electricity. Hydrogen can be provided from two sources: (1) a solar water electrolyzer and (2) a SCWG, which generates hydrogen from biomass gasification via hydrothermal conversion route. The SCWG uses water as the gasifying agent at its supercritical condition to decompose the organic biomass such as kitchen waste and organic biomass to hydrogen, carbon dioxide, carbon monoxide, and methane gas, allowing for the achievement of a very high volumetric hydrogen ratio. Moreover, SCWG can resolve some problems facing conventional biomass gasification. Among many hydrogen production methods, eco-friendly and high purity of hydrogen can be obtained by water electrolysis. Solar hydrogen production by alkaline water electrolysis was considered in this study as a most promising technique for high pure, efficient hydrogen production from renewable energy sources, which only emits oxygen as a byproduct without any carbon emissions. The proton-exchange membrane (PEM) fuel cell type was also considered due to its compact design, high efficiency, fast response, small footprint, and lower operating temperatures (20–80 °C), which makes it more suitable for residential applications.

The proposed system was used to minimize the mismatch between electricity demand and supply in a remote residential area located in Fukushima prefecture in Japan. The proposed HRES can offer co-benefits from enhancing both clean energy deployment and waste management strategies in the selected residential area. The overall configuration of the proposed HRES is shown in Figure 1.

The optimal designing of the proposed HRES beyond economic optimization will be discussed on the basis of conducting a techno-economic analysis, using the integrated simulation–optimization modeling framework. The model is employed to perform sensitivity analyses of the levelized cost of energy (LCOE) with respect to two scenarios: (1) off-grid system with limited biomass feedstock and (2) grid-tied system with the feed-in-Tariff (FiT) scheme.
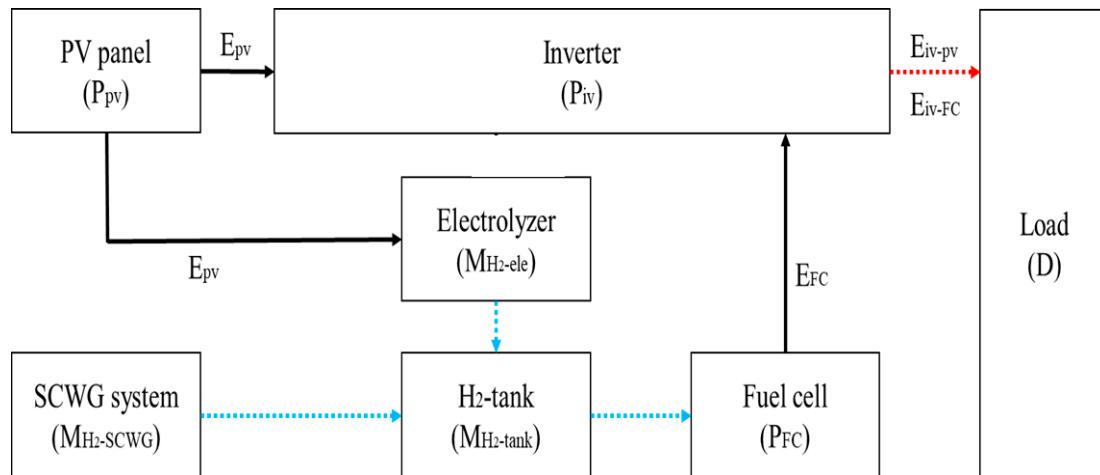
Figure 1. Proposed system configuration.

2. Simulation Model

2.1. PV Panel

The PV array output power can be calculated using the following formulas [26]:

$$P_{PV} = P_{max} F_{PV} \left(\frac{\overline{I_T}}{\overline{G_{T,\text{STC}}}} \right) \left[1 + \alpha_p (T_c - T_{c,STC}) \right] \tag{1}$$

$$T_c = T_a + G_T \left(\frac{T_{c,\,NOCT} - T_{a,\,NOCT}}{G_{T,NOCT}} \right) \left(1 - \frac{\eta_{cell}}{\tau\alpha} \right) \tag{2}$$

where P_{max} is the rated capacity of the PV panel (kW); F_{PV} is the PV derating factor, which is dependent on PV surface conditions such as clearness (%); $\overline{I_T}$ is the incident radiation to the PV surface (kW/m^2); $\overline{G_{T,\text{STC}}}$ is the incident radiation under standard conditions; α_p refers to the cell temperature coefficient (%/°C); T_c is the cell temperature; $T_{c,STC}$ is the PV cell temperature under standard conditions; T_a indicates the ambient temperature; $T_{c,\,NOCT}$ is the nominal operating cell temperature of the PV module; $T_{a,\,NOCT}$ is the ambient temperature at the NOCT (nominal operating cell temperature); and η_{cell} is cell efficiency which can be assumed to equal to the maximum power point efficiency η_{max}. The main input data used in Equations (1) and (2) are reported in Table 2.

Table 2. Main input data used in the PV output power estimation [27].

Parameter	Symbol	Value
Temperature coefficient (%/deg)	α_p	−0.258
Maximum efficiency	η_{max}	0.217
Rated power (W)	P_{max}	325
Nominal operation cell temperature (°C)	$T_{c,\,NOCT}$	44
Nominal operation ambient temperature (°C)	$T_{a,\,NOCT}$	20
Incident radiation under test condition (W/m^2)	$\overline{G_{T,STC}}$	1000
Derating factor	F_{PV}	0.9
Cell temperature under test condition (°C)	$T_{c,STC}$	25

The relationship between sun path and solar panel angel is depicted in Figure 2.
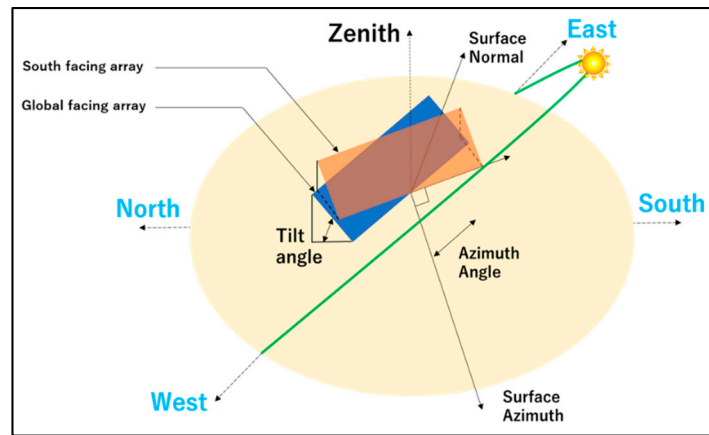
Figure 2. Relationship between sun path and solar panel.

The incident radiation to the PV surface is a function of the ambient condition, time, and period of the earth's revolution, which can be calculated by using the equation below [28]:

$$I_T = I_{grobal}\left\{\left(\cos\psi\cos\kappa + \sin\psi\sin\kappa\cos(\lambda - \zeta) + \mu\cos\frac{\psi}{2}\right) + \rho\left(\cos\kappa + \mu\sin^2\frac{\psi}{2}\right)\right\} \quad (3)$$

where I_{grobal} is global irradiance on a surface perpendicular to the vector of sunlight (kW/m^2); μ is diffuse portion constant for calculation of diffuse radiation as a part of incident radiation; ψ is the tilt angle between the ground, which is parallel to the horizon, and the PV panel; ρ is the reflection index that is dependent on grounding condition; and λ and ζ indicate sun azimuth on the celestial sphere and plate azimuth angle (radians east > 0 and west < 0). The sun's zenith angle, κ, is the angle between the sun's rays, and the perpendicularity to the horizontal plane can be calculated as follows:

$$\cos\kappa = \sin\delta\sin\gamma + \cos\delta\cos\gamma\cos\alpha \quad (4)$$

where δ is the solar declination angle on the celestial sphere, which is concerned sun altitude, and γ is the latitude in the observed point. The sun's declination is the angle between a line connecting the center of the sun and earth and the projection of this line on the equatorial plane. It varies between +23.45 and −23.45 degrees, which can be calculated by the following formula:

$$\delta = -23.45\cos\left(\frac{360}{365} \times (d + 10)\right) \quad (5)$$

where α is the solar angle, which is the angle between the run's ray and the projection of that ray on a horizontal surface, which can be calculated by using the following equations [29]:

$$\alpha = 360/24 \times (T - 12) \quad (6)$$

$$T = \text{Local Time} + \text{EOT} - 4L_{local} + 60T_{zone} \quad (7)$$

$$\text{EOT} = -9.87\sin 2N + 7.53\cos N + 1.5\sin N \quad (8)$$

$$N = \frac{360}{364} \times (d - 81) \quad (9)$$

where *d* is the day number when January 1 in each year is 1, and T is the solar time identified by Equation (7). *Local Time* is the local standard time in observed point, *EOT* is the equation of time to express the relationship of the earth's revolution speed around the sun (minutes), L_{local} is longitude in observed point, and T_{zone} is the time difference to GMT (Greenwich Mean Time). The calculation flow in the solar power simulation is shown in Figure 3.
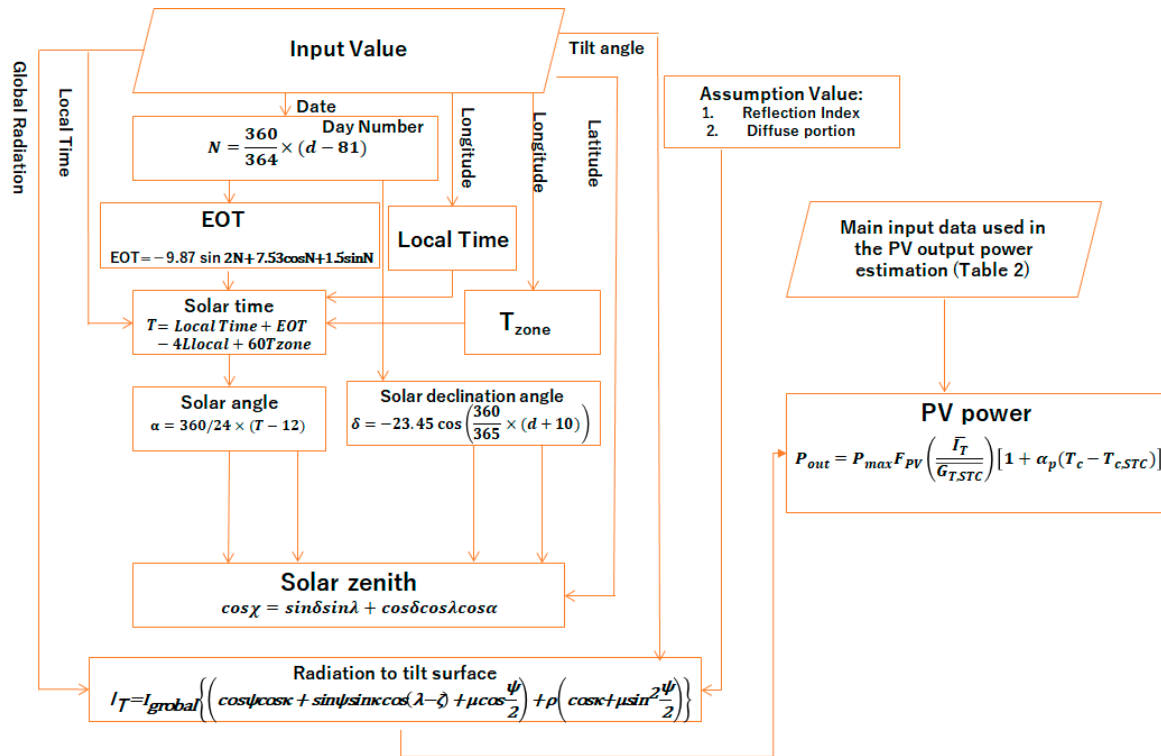
Figure 3. Calculation flow in solar power simulation.

2.2. Fuel Cell

The output power of the fuel cell, P_{FC}, is proportional to the rate of hydrogen consumption (m_{H_2}) [30]:

$$P_{FC} = N \cdot I_{FC} \cdot E_{FC} \tag{10}$$

where N is the number of cells, and I_{FC} is the current flow of cells [A]. E_{FC} refers to the electromotive energy of fuel cell [V], which is calculated as follows:

$$I_{FC} = \frac{2F}{N \cdot v \cdot M} \dot{m}_{H_2} \tag{11}$$

$$E_{FC}[V] = E_0 - b(\log(i)+3) - R_{ohmic}i - 0.000014e^{8i} \tag{12}$$

where F is the Faraday constant $\left[\frac{s\,A}{mol}\right]$; v is the stoichiometry of the reaction; M is the molecular mass of hydrogen $\left[\frac{g}{mol}\right]$; m_{H_2} is the rate of hydrogen consumption $\left[\frac{g}{s}\right]$; and i is the current flow density, which is a function of the reaction area (A) as follows:

$$i = I/A \tag{13}$$

$$b = \frac{1}{2} \frac{nF}{RT} \tag{14}$$

where n is the number of exchanged electrons in the reaction, T is the working temperature of fuel cells (°C), and R is the gas constant (J/mol·C). Generally, the range of working temperature of PEM (polymer electrode membrane) fuel cells is between 353.15 K (80 °C) to 393.15 K (120 °C). E_0 is the open-circuit voltage (OCV). This value is dependent on the working cell temperature. The ohmic loss in Equation (13) can be calculated by using the following equation:

$$R_{ohmic} = r_m L_{mem} \tag{15}$$

where r_m refers to the specific resistivity for the flow of hydrated protons (Ω cm), and L_{mem} is the thickness of the polymer membrane (cm) [31]. The input values of the technical parameters used in the above equations are reported in Table 3.

Table 3. Main input data used in the fuel cell simulation [31].

Parameter	Symbol	Value
Working temperature (°C)	T	80
Faraday's constant $\left(\frac{s\,A}{mol}\right)$	F	96,485
Reaction area (cm^2)	A	1000
Number of cells	n	82
Thickness of the polymer membrane (μm)	L_{mem}	125
Specific resistivity (Ω cm)	r_m	0.1
Stoichiometry of the reaction	υ	1
Open-circuit voltage (V)	E_0	1.17
Molecular mass of hydrogen $\left(\frac{g}{mol}\right)$	M	2

The calculation flow used in the simulation of the fuel cell is shown in Figure 4.
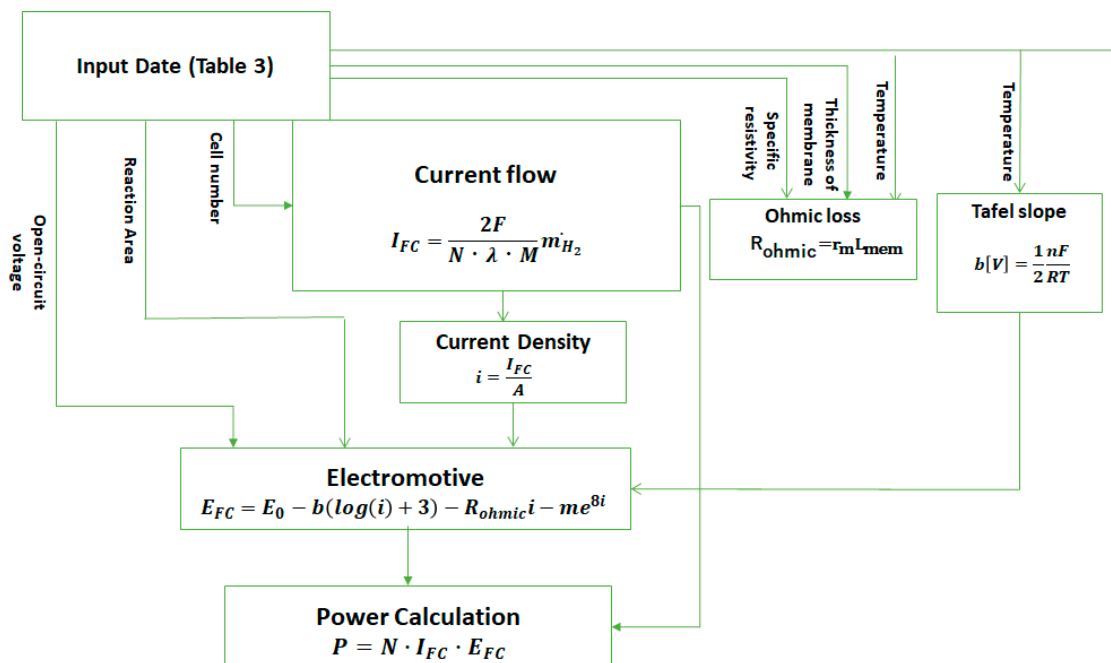
Figure 4. Calculation flow in fuel cell power simulation.

2.3. Electrolyzer

In a water electrolyzer, water is decomposed into hydrogen and oxygen by using electricity. The electricity consumption (Elec$_{EL}$) of the electrolyzer is identified as a function of rated hydrogen flowrate ($Q_{n\text{-}H2}$) and actual hydrogen flowrate (Q_{H2}) [32]:

$$\text{Elec}_{EL} = A_E Q_{n-H_2} + B_E Q_{H_2} \tag{16}$$

where $A_E = 20$ (kWh/kg) and $B_E = 40$ (kWh/kg) are the electricity consumption curve coefficients of the electrolyzer, which were collected from [15].

2.4. Hydrogen Tank

The following equation expresses the state of charge of the hydrogen storage tank:

$$H_{2_{level}}(t) - H_{2_{level}}(t-1) = M_{H_2-ele}(t) + M_{H_2-SCWG}(t) - M_{H_2-tank}(t) \; / \; \eta_{H_2-tank} \tag{17}$$

where M_{H_2-ele} and M_{H_2-SCWG} represent the inlet hydrogen flow rate from the electrolyzer and SCWG, respectively. η_{H_2-tank} is hydrogen tank efficiency, which is set at 80%. The hydrogen tank has the minimum H_{2-min} and the maximum H_{2-max} of levels that are set at 5% and 90%, respectively.

2.5. SCWG

The K-value model was used to determine the species and their amounts of the biomass supercritical gasification reaction in the equilibrium state at a specific temperature and pressure, which is expressed by the following equation:

$$K_i = \prod_{j=1}^{N} a_j^{v_j} \tag{18}$$

Here, the biomass feedstock is considered as kitchen garbage and food waste with a moisture content of 40% and a mass composition of C = 48%, H = 6.4%, and O = 37.6%. The assumed basic kinetic reactions that take place in a typical SCWG reactor are represented as follows:

$$C_cH_xO_y + wH_2O \rightarrow x_1CO + x_2H_2 + x_3CO_2 + x_4H_2O + x_5CH_4 \tag{19}$$

where c, x, and y are given as mole fractions of the biomass feedstock such as glucose. w refers to the mass flow rate of water used in the gasification reaction. The element balances of carbon, hydrogen, and oxygen elements are given below:

$$x_1 + x_3 + x_5 - c = 0 \tag{20}$$

$$x + 2w - 2x_2 - 2x_4 - 4x_5 = 0 \tag{21}$$

$$y + w - x_1 - 2x_3 - x_4 = 0 \tag{22}$$

where x_1 to x_5 show the stoichiometric number of each substance. Two more equations would be needed to solve the above system of equations, which can be adjusted, using the definition of the constant of the equilibrium constant, K, as follows:

$$K_1 = \frac{x_{H_2}x_{CO_2}}{x_{H_2O}x_{CO}} \tag{23}$$

$$K_2 = \frac{x_{CH_4}}{\left(x_{H_2}\right)^2} \tag{24}$$

The values of K_1 and K_2 are dependent on the reaction temperature, which at the supercritical condition can be expressed as follows [33]:

$$lnK_1 = \frac{7082.848}{T} + (-6.567)lnT + \frac{7.466 \times 10^{-3}}{2}T + \frac{-2.164 \times 10^{-6}}{6}T^2 + \frac{0.701 \times 10^{-5}}{2T^2} + 32.541 \tag{25}$$

$$lnK_2 = \frac{5870.53}{T} + 1.86lnT - 2.7 \times 10^{-4}T + \frac{58200}{T^2} - 18.007 \tag{26}$$

3. Design of the Proposed HRES beyond Economic Optimization

3.1. Optimization Problem

To design a highly efficient HRES, priority should be given to sizing the system components. An optimization model is developed here to obtain the optimum size or the optimal configuration of the proposed HRES (Figure 1). The optimum sizing method can help to guarantee the lowest investment with full use of the HRES, so that it can work at the optimum conditions in terms of investment and system reliability. The decision variables in the optimization process are the capacity of each power generator and the storage component of the HRES. The optimization criterion can be defined on the basis of the minimization of the total cost of the system or maximization of the total revenue achieved from the generated electricity, subject to satisfying the demand load requirements. On the basis of the mode of power generation from the HRES, the optimization problems listed below were introduced in this research.

3.1.1. Off-Grid Operation Mode

The optimal design of the off-grid HRES was based on the minimization of the total cost of the system:

$$\text{Total Cost} = \sum_i \text{LCOE}_i \times \text{E}_i \tag{27}$$

where E_i indicates the amount of electricity generated by each component i (i.e., PV panel and fuel cell) (kWh). *LCOE* is the levelized cost of electricity generated by the HRES (JPY/kWh), which is calculated as follows:

$$\text{LCOE}_i = \frac{\sum_{t=1}^{n}(\text{I}_{it}+\text{M}_{it})/(1+\text{r})^t}{\sum_{t=1}^{n}\text{E}_{it}/(1+\text{r})^t} \tag{28}$$

where I_{it} and M_{it} refer to the investment and operation costs of each component i in year t (JPY/Y), respectively. n indicates the lifetime of the system.

3.1.2. Grid-Tied Operation Mode

The profit maximization problem describes the situation wherein the surplus electricity generated from the solar panel can be sold back to the grid, which can be defined as follows:

$$\text{Profit} = \alpha \text{E}_{\text{dem}} + \beta \text{E}_{\text{sur}} - \text{Total Cost} \tag{29}$$

where α is the average price of electricity in Japan, which is equal to 26 JPY/kWh [34]; E_{dem} is the demand for electricity in the selected household area, which is met by the HRES (kWh); β is FiT (Feed-in-Tariff), which is equal to 28 JPY/kWh [34]; and E_{sur} is surplus electricity generated by the PV panel (kWh).

3.2. Demand Constraint

The main goal in the scenarios above (cost minimization/profit maximization) is to find the optimal configuration of the proposed system subject to satisfying the hourly electricity demand–supply balance in the selected household area, considering the following constraint:

$$\text{E}_{\text{FC}}(\text{h}) + \text{E}_{\text{PV}}(\text{h}) = \text{E}_{\text{dem}}(\text{h}) \tag{30}$$

where E_{pv} and E_{FC} refer to the amount of electricity generated from the PV panel and the fuel cell in each timestep h, respectively.

3.3. Solving Method

PSO (particle swarm optimization) algorithm is one of the meta-heuristic algorithms used to find the approximate solution in the case of a combinatorial optimization problem [35–37]. The behavior of this algorithm comes from the characteristic of collective organisms. Under giving the objective function as the searching target, particles move around with information communication in searching space to find the optimal solution. This method, which consists of a constant search of the best solution, moves the particles at a specific speed calculated in each iteration. The expected result is that the particle swarm converges to the best solution. Particle motions are defined by a vector, which represents the velocity of the swarm in each direction. The velocity and position for each swarm are updated according to its experience and the best global particle. PSO was used to find the optimal size of the main components of the proposed HRES. Figure 5 shows the connection between the optimization and the simulation parts. The simulation part can calculate the hourly hydrogen and electricity generation over a year, given the demand load requirement and weather conditions (temperature and global radiation). The fitness values of the PSO algorithm are the installed capacity of each component of HRES such as PV module, fuel cell, electrolyzer, hydrogen tank, and SCWG reactor. The estimated fitness values were checked with the simulation part to ensure that the HRES meets the annual electricity balance. If the goal was not achieved, the PSO algorithm would find another fitness value by updating the velocity and position of each particle, using the following equations:

$$v_{id}(t+1) = \omega \cdot v_{id}(t) + c_1 \cdot \phi_1 \cdot (P_{id}(t) - x_{id}(t)) + c_2 \cdot \phi_2 \cdot (g_{id}(t) - x_{id}(t)) \tag{31}$$

$$x_{id}(t+1) = x_{id}(t) + v_{id}(t+1) \tag{32}$$

where $v_{id}(t+1)$ is particle vector after updating; $v_{id}(t)$ is particle vector before updating; and ω is inertia weight of vectors, which control the vector size—this value should be selected from 0.5 to 1 [38]. Here, ω is set as 0.7. The values of C_1 and C_2 are set as 1.0 and 0.5, respectively [39].
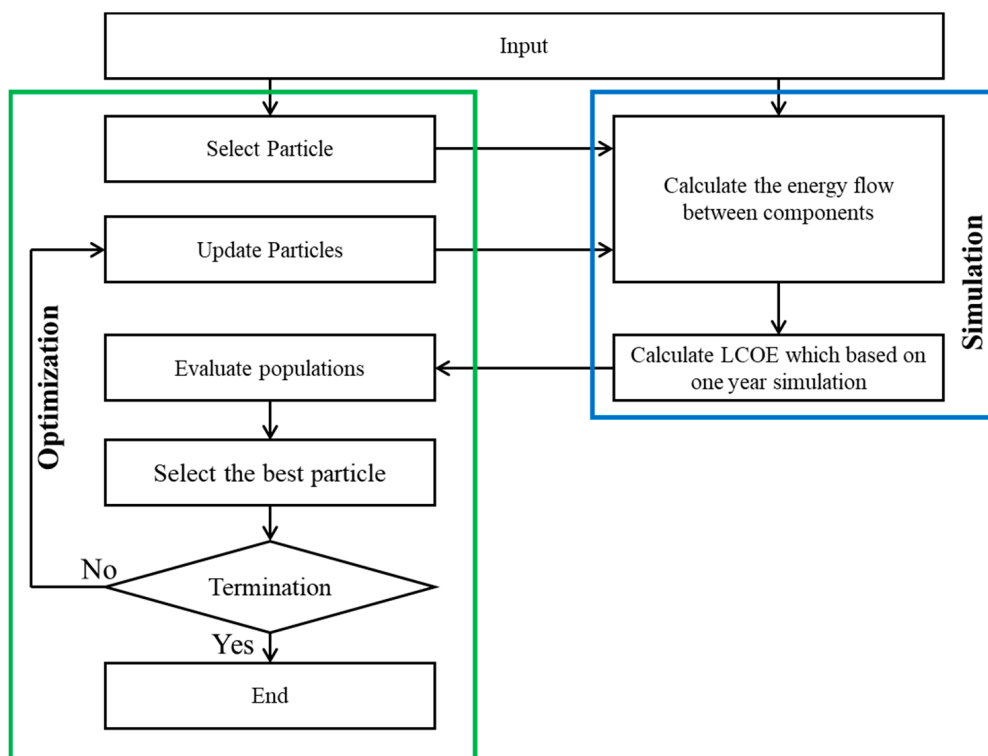

Figure 5. The connection between the optimization and simulation parts. Adopted from [40].

4. Results and Discussion

4.1. Case Study

The proposed HRES was utilized in a residential area located in a subject district in Shinchi-machi of Fukushima prefecture, Japan. The hourly load curves for a typical household located in the selected residential area is shown in Figure 6 [41]. As can be observed from this figure, the first ramp takes place between 5:00 a.m. and 8:00 a.m. when people are starting to work in the morning, followed with the second ramp between 4:00 p.m. and 8:00 p.m. when people are getting back to their homes in the evening. Furthermore, the amount of electricity consumption is much higher during winter-time, since the demand for space heating increases. The average annual electricity demand in the selected household was estimated at 4.37 MWh.
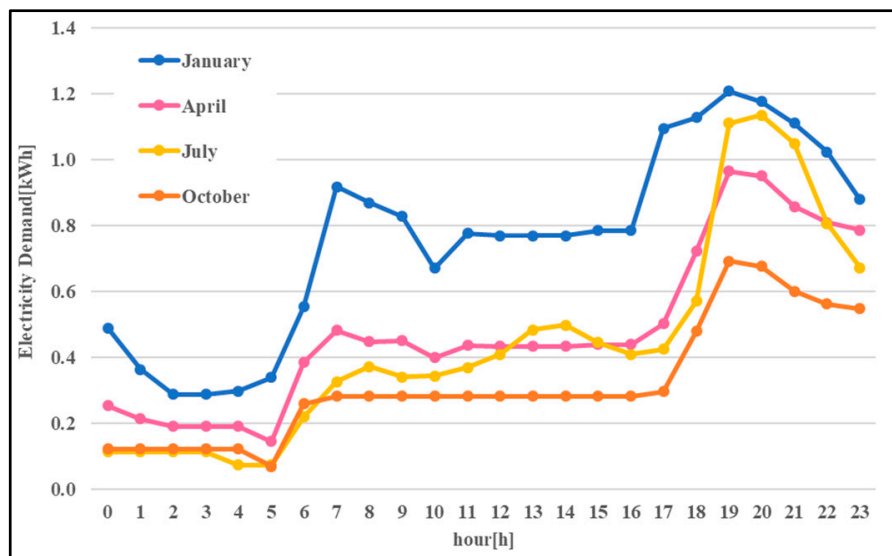
Figure 6. Electricity demand for a typical Japanese household.

The ambient temperature and average global irradiation in Fukushima were collected from the Japan Meteorological Agency (JMA) throughout the entire period in 2019, which is shown in Figures 7 and 8 [42]. From April to June, the global radiation had the highest value. In August, the global radiation decreased slightly. Because this region is affected by seasonal wind, the weather condition in this area, especially in summer, is variable.

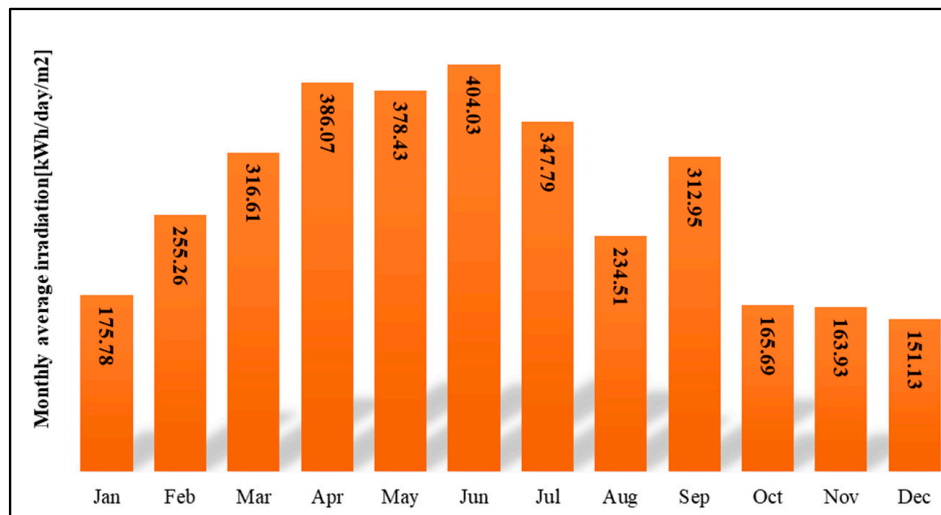**Figure 7.** Monthly average temperature in Fukushima.

Figure 8. Monthly average solar irradiation in Fukushima.

4.2. Cost Analysis of the HRES

PV module: The installation cost of the PV module was assumed to be 230 JPY/W for the residential rooftop, and the annual operation and maintenance cost was estimated at 5% of the installation cost with a lifetime of 20 years [43,44].

Electrolyzer: The alkaline electrolyzer was selected in this study with a total lifetime of 10 years. The installation cost of the alkaline water-electrolyzer was estimated at 170 JPY/W [45], together with an annual operation and maintenance cost of 3 JPY/W [45].

Fuel cell: The installation cost for the fuel cell was estimated at 400 JPY/W with a total lifetime of 10 years [45]. The operation and maintenance cost of the PEM fuel cell was considered at 1% of the installation cost.

Hydrogen tank: The installation cost of a hydrogen tank was estimated at 150,000 JPY/ kg_{H2} with a total lifetime of 20 years, together with operation and maintenance costs of 9000 JPY/year.

SCWG reactor: The unit cost of the SCWG reactor is estimated on the basis of the amount of the biomass feedstock, which can be processed in the reactor. In this research, it was approximated around 42,000 JPY/($kg_{feedstock}$/day) [9]. The hydrogen production cost of the SCWG was estimated at 610 JPY/kg_{H2} [46]. This value is much higher than the hydrogen production cost of conventional methods, such as natural gas reforming, which is about 140 JPY/kg_{H2} [47].

4.3. Scenario Analysis

4.3.1. Scenario 1: Off-Grid System with Limited Biomass Feedstock

The total amount of annual food waste from the household sector in Japan is estimated at about 6.46 million tons [48]. Considering Japan population in 2019, which was about 126.2 million, the total kitchen and food waste produced by each inhabitant can be calculated by about 51.2 (kg/year). Take into consideration this assumption that at four dwellers living in each household, the quantity of the annual food waste from one Japanese family is approximated at 204.7 (kg/year), which can be used in the SCWG. The results of this scenario are reported in Table 4. The annual electricity demand in the selected household can be met by a combination of solar electricity generation (39%) and fuel cell electricity generation (61%). The hourly electricity supply–demand in this scenario is represented in Figure 9.

Since the amount of annual biomass feedstock is limited in this scenario, the required hydrogen for feeding the fuel cell should therefore be provided by the solar electrolyzer. During the cold seasons, the demand for hydrogen increases for the fuel cell, and therefore the SCWG has the pivotal role as the optional function for hydrogen generation, which is basically due to lack of solar electricity generation

during this period. Since the amount of annual kitchen waste generated from one household is limited, additional sources of wet biomass such as sewage sludge from the nearby commercial buildings should therefore be considered in this scenario. Figure 10 shows the monthly average electricity generation from the proposed HRES in this scenario. In the winter season, the amount of the generated electricity from the fuel cell was found to be higher than the other seasons. This was because the demand for electricity in winter-time is very high, and the electricity generated from the PV module was not enough due to insufficient solar irradiation. The monthly hydrogen production from the solar electrolyzer and SCWG is shown in Figure 11.

Table 4. Optimal configuration of the proposed HRES in scenario 1.

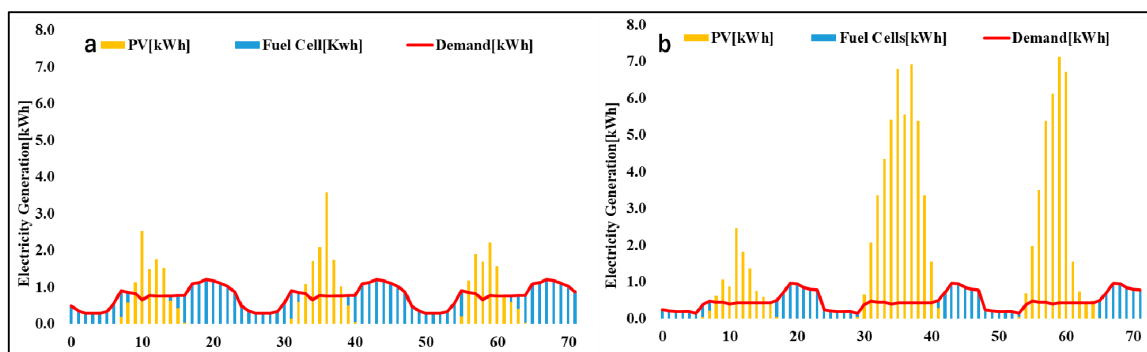| PV Panel (kW)	FC (kW)	Electrolyzer (kW)	Hydrogen Tank (kg)	SCWG (kg/h)
8	1.5	1.5	5	1

Figure 9. Hourly simulation of the electricity supply/demand in scenario 1: (**a**) January 1–January 4; (**b**) April 1–April 4).

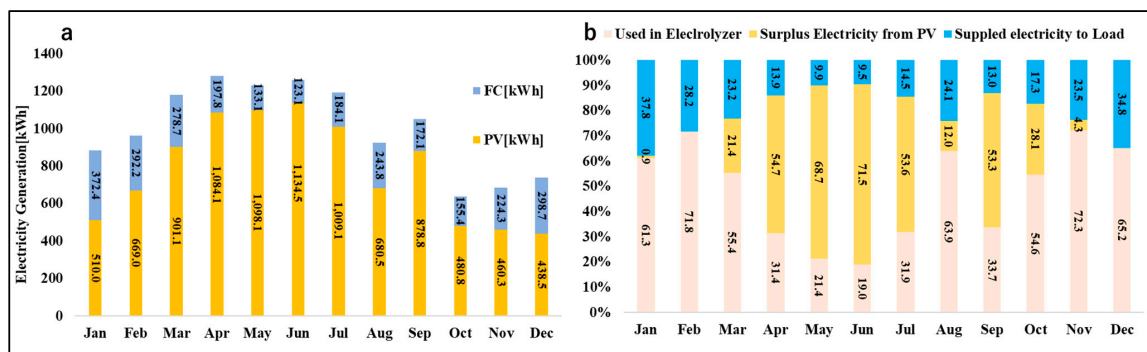**Figure 10.** Monthly average electricity supply and demand in scenario 1: (**a**) total electricity generation from the HRES; (**b**) usage of the total electricity.
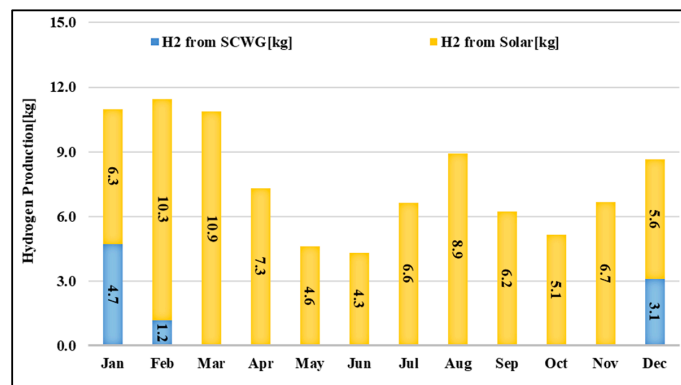

Figure 11. Monthly average hydrogen production in scenario 1.

The optimal solution in this scenario was obtained at the discounted annual cost of 244,550 JPY/year. The LCOE was estimated at 55.92 JPY/kWh in this scenario. The size of the solar electrolyzer increased extremely in order to provide a sufficient amount of hydrogen for the fuel cell. Figure 12 shows the PSO process through the swarm's motion in different iterations from 0 to 20 in this scenario. It can be seen that particles (PV, fuel cell, and SCWG) flew from random initialization toward the particle best and global best so that all the particles converged to one point, which is called global best. The particles met each other after 20 iterations within an objective domain from 0 to 5.
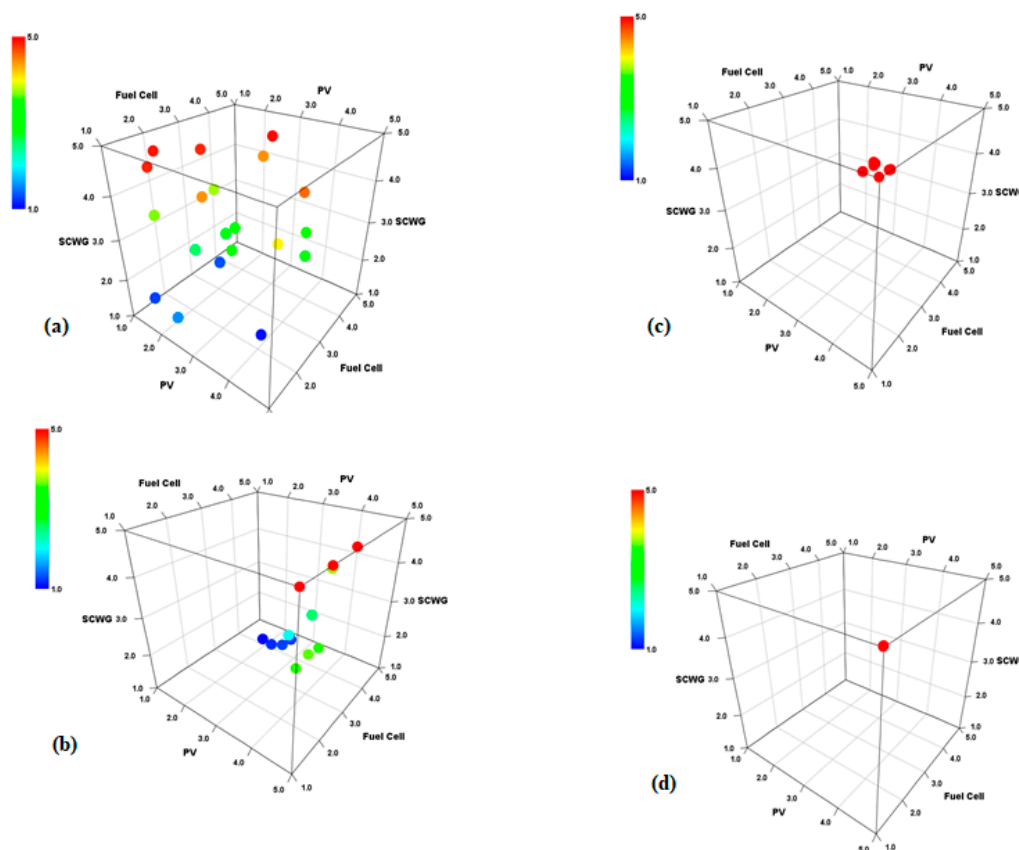
Figure 12. Particle positions (PV vs. fuel cell vs. SCWG) in different iterations: (**a**) = 0, (**b**) = 3, (**c**) = 9, (**d**) = 20.

### 4.3.2. Scenario 2: Grid-tied System Considering the FiT Scheme

On the basis of this scenario, the total revenue from deploying the proposed HRES can be derived from two ways: (1) by replacing the total purchased electricity that is needed to meet the load requirement with the electricity generated by the HRES, and (2) selling back the surplus electricity generated by the PV panel to the grid, considering the FiT scheme. The optimal configuration of the HRES in this scenario is reported in Table 5. The model estimates the annualized total cost of the system at 262,100 JPY/year. The LCOE was calculated at 59.93 JPY/kWh, which can guarantee a net profit of 15,140 JPY/year for the system.

Table 5. Optimal configuration of the proposed HRES in scenario 2.

| PV Panel (kW)	FC (kW)	Electrolyzer (kW)	Hydrogen Tank (kg)	SCWG (kg/h)
10	1.5	1.5	5	1

In order to provide a sufficient amount of hydrogen for the fuel cell, both sizes of the SCWG reactor and PV panel will increase. To obtain the maximum profit, the first priority is given to the

SCWG to provide enough hydrogen and fill the hydrogen tank. Therefore, the surplus solar electricity would be available for selling back to the grid, which will result in increasing the net profit. In this scenario, the total size of the PV panel for the residential application was limited to 10 kW. The hourly electricity supply–demand in this scenario is represented in Figure 13.
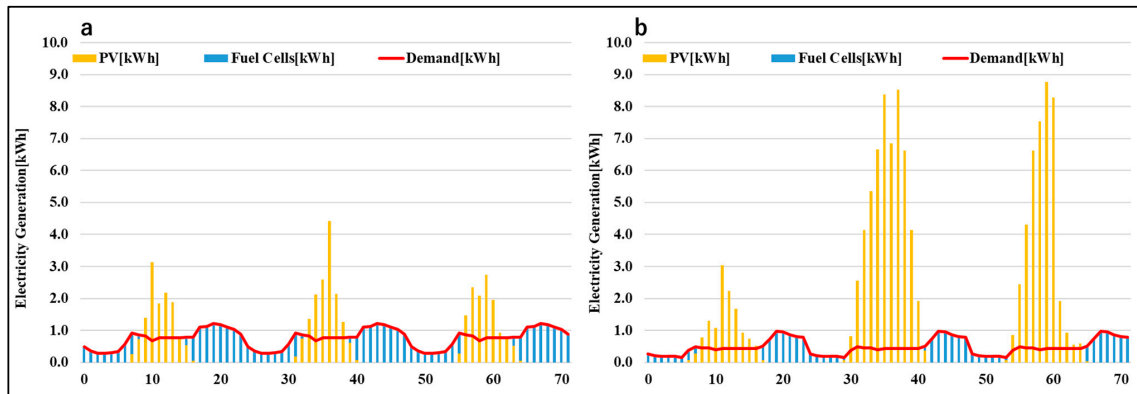

Figure 13. Hourly simulations of the electricity supply/demand in scenario 2: (**a**) January 1–January 4; (**b**) April 1–April 4.

During the winter season, the share of surplus electricity was around 0–1%, which is negligible due to the severe weather conditions and higher demand for electricity in the selected residential area. During the summer and spring seasons, the need for electricity decreases, and therefore the HRES will be able to supply more surplus electricity to the grid. The monthly average electricity and hydrogen generation from the proposed HRES are shown in Figures 14 and 15, respectively.
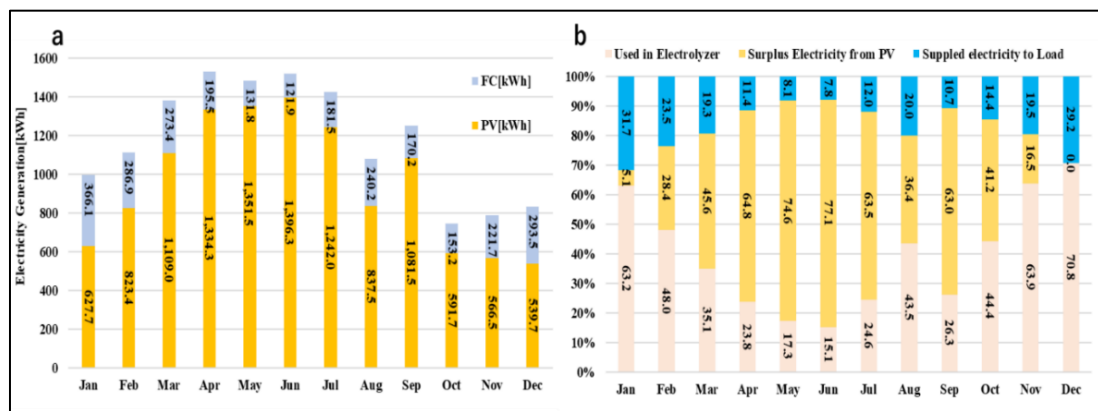
Figure 14. Monthly average electricity supply and demand in scenario 2: (**a**) total electricity generation from the HRES; (**b**) usage of the total electricity.
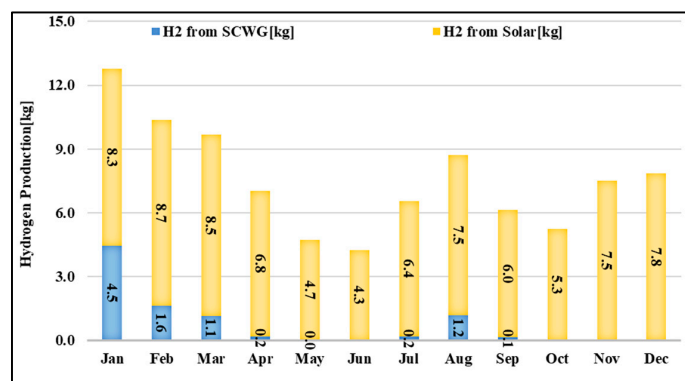
Figure 15. Monthly average hydrogen production in scenario 2.

The results of the techno-economic analysis model for the two scenarios are summarized in Table 6. The comparison between scenario 1 and scenario 2 highlighted the role of the PV module in increasing the profit through selling back the surplus electricity to the grid, using the FiT mechanism. The estimated value of LCOE in scenario 1 was less than its value in scenario 2, which indicates the superiority of the cost minimization problem over the profit maximization problem for this particular case study in which access to biomass feedstock was limited.

Table 6. Techno-economic analysis results for the two scenarios.

Scenarios	Power Mix (%)		Annual Hydrogen Production Mix (%)		Annual Biomass Consumption (kg)	Total Cost (JPY/year)	LCOE (JPY/kWh)	LCOE, Including the Annual Profit (JPY/year)
	PV	FC	PV	SCWG				
Scenario 1	78	22	90	10	264.3	¥244,550	¥55.92	-
Scenario 2	81	19	90	10	264.3	¥262,100	¥59.93	¥56.47

5. Conclusions

In this study, modeling and simulation of a hydrogen-based HRES were conducted in order to find the optimal configuration of the system that can be used to meet the electrical load requirement of a typical Japanese household located in a residential area in Shinchi-machi, Fukuoka prefecture, Japan.

The modeling framework was developed using both the cost minimization and profit maximization approaches. The simulation part was developed to estimate the hourly electrical power generated by the proposed HRES, taking into account the variation of the weather parameters and given the demand load. The optimization model's main goal was set to find the optimal configuration of the system subject to satisfying the required demand load, considering two scenarios: (1) minimization of the total cost of the system in an off-grid mode and (2) maximization of the total profit obtained from using renewable electricity and selling surplus solar electricity to the grid, considering the feed-in-tariff (FiT) scheme in a grid-tied mode. As indicated by the model results, the proposed HRES could generate about 47.3 MWh of electricity in all scenarios, which was needed to meet the external load requirement in the selected study area. The LCOE of the system in scenarios 1 and 2 was estimated at 55.92 JPY/kWh and 56.47 JPY/kWh, respectively. Comparison between scenario 1 and scenario 2 showed that the capacity of electrolyzer and PV module with limited biomass feedstock increases. The limited availability of biomass feedstock resulted in increasing the share of the PV panels and decreasing the share of the fuel cell in the total supply mix. The results of the profit maximization problem revealed the role of the PV module in increasing the profit by selling back the surplus electricity to the grid, using the FiT mechanism. Therefore, the reduction of the cost of the solar-hydrogen system turned out to be by far the most critical cost driver under the profit maximization scenario, when the FiT system was enforced.

However, the big challenge facing residential HRES that we discussed in this paper is their economic viability and cost-effectiveness. Rather, cost-conscious policymakers often remain reluctant to invest financial resources in this area. Despite limited incentives provided by the local governments such as feed-in-tariff and J-Credit to compensate for the capital investments of a number of large-scale commercial and independent power producers, there are no major regulatory efforts that have focused specifically on the promotion of the hybrid residential microgrids in Japan. Providing long-term policies and effective incentive strategies leads to the widespread deployment of residential microgrids in the whole country. The demonstration programs such as those we discussed in this paper will help the government to set long-term goals and an initial foundation for microgrid development in cities. On the basis of the detailed technical insights obtained from this study, the economic benefits of the proposed HRES for customers, utilities, and society can be evaluated, and then policies can be implemented to ensure the hybrid residential microgrid owner receives incentives or other support to monetize those benefits.

References

1. McLellan, B.C.; Zhang, Q.; Utama, N.A.; Farzaneh, H.; Ishihara, K.N. Analysis of Japan's post-Fukushima energy strategy. *Energy Strategy Rev.* **2013**, *2*, 190–198. [CrossRef]

2. Esteban, M.; Portugal-Pereira, J.; Mclellan, B.C.; Bricker, J.; Farzaneh, H.; Djalilova, N.; Ishihara, K.N.; Takagi, H.; Roeber, V. 100% renewable energy system in Japan: Smoothening and ancillary services. *Appl. Energy* **2018**, *224*, 698–707. [CrossRef]

3. Farzaneh, H. *Devising a Clean Energy Strategy for Asian Cities*; Springer: Berlin/Heidelberg, Germany, 2018.

4. Elliott, D.C. Catalytic hydrothermal gasification of biomass. *Biofuels Bioprod. Biorefining* **2008**, *2*, 254–265. [CrossRef]

5. Jessop, P.G.; Ikariya, T.; Noyori, R. Homogeneous catalysis in supercritical fluids. *Chem. Rev.* **1999**, *99*, 475–494. [CrossRef] [PubMed]

6. Modell, M. Reforming of glucose and wood at critical conditions of water. *Mech. Eng.* **1977**, *99*, 108.

7. Savage, P.E. A perspective on catalysis in sub- and supercritical water. *J. Supercrit. Fluids* **2009**, *47*, 407–414. [CrossRef]

8. Reddy, S.N.; Nanda, S.; Dalai, A.K.; Kozinski, J.A. Supercritical water gasification of biomass for hydrogen production. *Int. J. Hydrogen Energy* **2014**, *39*, 6912–6926. [CrossRef]

9. Farzaneh, H. Design of a hybrid renewable energy system based on supercritical water gasification of biomass for off-grid power supply in Fukushima. *Energies* **2019**, *12*, 2708. [CrossRef]

10. Chang, P.; Hsu, C.; Hsiung, C.; Lin, C. Constructing an innovative bio-hydrogen integrated renewable energy system. *Int. J. Hydrogen Energy* **2013**, *38*, 15660–15669. [CrossRef]

11. Sharafi, M.; ELMekkawy, T.Y. Multi-objective optimal design of hybrid renewable energy systems using PSO-simulation based approach. *Renew. Energy* **2014**, *68*, 67–79. [CrossRef]

12. Sen, R.; Bhattacharyya, S.C. Off-grid electricity generation with renewable energy technologies in India: An application of HOMER. *Renew. Energy* **2014**, *62*, 388–398. [CrossRef]

13. Mohammed, O.H.; Amirat, Y.; Benbouzid, M. Particle swarm optimization of a hybrid wind/Tidal/PV/Battery energy system. Application to a remote area in bretagne, France. *Energy Procedia* **2019**, *162*, 87–96. [CrossRef]

14. Giannakoudis, G.; Papadopoulos, A.I.; Seferlis, P.; Voutetakis, S. Optimum design and operation under uncertainty of power systems using renewable energy sources and hydrogen storage. *Int. J. Hydrogen Energy* **2010**, *35*, 872–891. [CrossRef]

15. Dufo-López, R.; Bernal-Agustín, J.L. Multi-objective design of PV–wind–diesel–hydrogen–battery systems. *Renew. Energy* **2008**, *33*, 2559–2572. [CrossRef]

16. Abedi, S.; Alimardani, A.; Gharehpetian, G.; Riahy, G.; Hosseinian, S. A comprehensive method for optimal power management and design of hybrid RES-based autonomous energy systems. *Renew. Sustain. Energy Rev.* **2012**, *16*, 1577–1587. [CrossRef]

17. Amer, M.; Namaane, A.; M'Sirdi, N. Optimization of hybrid renewable energy systems (HRES) using PSO for cost reduction. *Energy Procedia* **2013**, *42*, 318–327. [CrossRef]

18. Sawle, Y.; Gupta, S.; Bohre, A.K. Optimal sizing of standalone PV/wind/biomass hybrid energy system using GA and PSO optimization technique. *Energy Procedia* **2017**, *117*, 690–698. [CrossRef]

19. Ozgoli, H.A.; Ghadamian, H.; Farzaneh, H. Energy efficiency improvement analysis considering environmental aspects in regard to biomass gasification PSOFC/GT power generation system. *Procedia Environ. Sci.* **2013**, *17*, 831–841.

20. Ghadamian, H.; Hamidi, A.A.; Farzaneh, H.; Ozgoli, H.A. Thermo-economic analysis of absorption air cooling system for pressurized solid oxide fuel cell/gas turbine cycle. *J. Renew. Sustain. Energy* **2012**, *4*, 043115. [CrossRef]

21. Rokni, M. Biomass gasification integrated with a solid oxide fuel cell and stirling engine. *Energy* **2014**, *77*, 6–18. [CrossRef]

22. Doherty, W.; Reynolds, A.; Kennedy, D. Computer simulation of a biomass gasification-solid oxide fuel cell power system using aspen plus. *Energy* **2010**, *35*, 4545–4555. [CrossRef]

23. Toonssen, R.; Aravind, P.V.; Smit, G.; Woudstra, N.; Verkooijen, A.H. System study on hydrothermal gasification combined with a hybrid solid oxide fuel cell gas turbine. *Fuel Cells* **2010**, *10*, 643–653. [CrossRef]

24. Farzaneh, H.; Ghalee, I.; Dashti, M. Simulation of a multi-functional energy system for Cogeneration of steam, power and hydrogen in a coke making plant. *Procedia Environ. Sci.* **2013**, *17*, 711–718. [CrossRef]

25. Moghadasi, M.; Ghadamian, H.; Farzaneh, H.; Moghadasi, M.; Ozgoli, H.A. CO_2 capture technical analysis for gas turbine flue gases with complementary cycle assistance including nonlinear mathematical modeling. *Procedia Environ. Sci.* **2013**, *17*, 648–657. [CrossRef]

26. Rosa, A.V. *Fundamentals of Renewable Energy Processes*; Academic Press: Cambridge, MA, USA, 2009.

27. Panasonic Panasonic Photovoltaic Module HITVBHN245SJ25VBHN240SJ25. Available online: https://panasonic.net/lifesolutions/solar/download/pdf/VBHN245_240SJ25_ol_190226.pdf (accessed on 14 January 2020).

28. Das, B.K.; Hoque, N.; Mandal, S.; Pal, T.K.; Raihan, M.A. A techno-economic feasibility of a stand-alone hybrid power generation for remote area application in Bangladesh. *Energy* **2017**, *134*, 775–788. [CrossRef]

29. Al-Waeli, A.H.A.; Kazem, H.A.; Chaichan, M.T.; Sopian, K. *Photovoltaic/Thermal (PV/T) Systems*; Springer–International Publisher Science, Technology, Medicine: Cham, Switzerland, 2019.

30. O'Hayre, R.; Cha, S.; Colella, W.; Prinz, F.B. *Fuel Cell Fundamentals*; John Wiley & Sons: Hoboken, NJ, USA, 2016.

31. Laoun, B.; Naceur, M.W.; Khellaf, A.; Kannan, A.M. Global sensitivity analysis of proton exchange membrane fuel cell model. *Int. J. Hydrogen Energy* **2016**, *41*, 9521–9528. [CrossRef]

32. Kashefi Kaviani, A.; Riahy, G.; Kouhsari, S. Optimal design of a reliable hydrogen-based stand-alone wind/PV generating system, considering component outages. *Renew. Energy* **2009**, *34*, 2380–2390. [CrossRef]

33. Castello, D.; Fiori, L. Supercritical water gasification of biomass: A stoichiometric thermodynamic model. *Int. J. Hydrogen Energy* **2015**, *40*, 6771–6781. [CrossRef]

34. The Electric Power Industry in Japan. (2020). Retrieved from Japan Electric Power Information Center Website. Available online: https://www.jepic.or.jp/pub/pdf/epijJepic2020.pdf (accessed on 14 January 2020).

35. Farzaneh, H. *Energy Systems Modeling: Principles and Applications*; Springer: Berlin/Heidelberg, Germany, 2019.

36. Farzaneh, H.; McLellan, B.; Ishihara, K.N. Toward a CO2zero emissions energy system in the Middle East region. *Int. J. Green Energy* **2014**, *13*, 682–694. [CrossRef]

37. Farzaneh, H.; Doll, C.N.; Puppim de Oliveira, J.A. An integrated supply-demand model for the optimization of energy flow in the urban system. *J. Clean. Prod.* **2016**, *114*, 269–285. [CrossRef]

38. Parsopoulos, K.; Vrahatis, M. Particle swarm optimization method for constrained optimization problem. In *Intelligent Technologies—Theory and Applications: New Trends in Intelligent Technologies*; IOS Press (Frontiers in Artificial Intelligence and Applications): Fairfax, VA, USA, 2002; Volume 76, pp. 214–220.

39. Zhang, W.J.; Xie, X.F.; Bi, D.C. Handling boundary constraints for numerical optimization by particle swarm flying in periodic search space. In Proceedings of the 2004 Congress on Evolutionary Computation, Portland, OR, USA, 19–23 June 2004; Volume 2, pp. 2307–2311.

40. Yoshida, Y.; Farzaneh, H. Optimal design of a stand-alone residential hybrid Microgrid system for enhancing renewable energy deployment in Japan. *Energies* **2020**, *13*, 1737. [CrossRef]

41. Japan Agency for National Resource and Energy. Available online: https://www.enecho.meti.go.jp/index.html (accessed on 14 December 2019).

42. Japan Meteorological Agency. Available online: https://www.data.jma.go.jp/obd/stats/etrn/view/monthly_s3_en.php?block_no=47401&view=11 (accessed on 14 December 2019).

43. Panasonic, Panasonic Residential Catalog. Available online: https://sumai.panasonic.jp/catalog/solarsystem.html (accessed on 10 December 2018).

44. Mohd, A.M.R.; Nasrudin, A.R.; Che, H.S.; Ohgaki, H.; Farzaneh, H.; Wallace, S.H.W.; Lai, C.H. Optimal solar powered system for long houses in sarawak by using HOMER tool. *Asean Eng. J.* **2019**, *9*, 2586–9159.

45. Hydrogen and Fuel Cellsin Japan. (2019). Retrieved from EU-Japan Centre for Industrial Cooperation Website. Available online: https://www.eu-japan.eu/sites/default/files/publications/docs/hydrogen_and_fuel_cells_in_japan.pdf (accessed on 14 January 2020).

46. Lu, Y.; Zhao, L.; Guo, L. Technical and economic evaluation of solar hydrogen production by supercritical water gasification of biomass in China. *Int. J. Hydrogen Energy* **2011**, *36*, 14349–14359. [CrossRef]

47. Hydrogen Production Tech Team Roadmap. (2017). Department of Energy. Available online: https://www.energy.gov/sites/prod/files/2017/11/f46/HPTT%20Roadmap%20FY17%20Final_Nov%202017.pdf (accessed on 14 January 2020).

48. Japan Costumer Affairs Agency. (5 April 2020). Policy Planning. Available online: https://www.caa.go.jp/en/policy/consumer_policy (accessed on 14 January 2020).